International Journal of Biological Macromolecules 264 (2024) 130448

Contents lists available at ScienceDirect

International Journal of Biological Macromolecules

journal homepage: www.elsevier.com/locate/ijbiomac

Cellulose de-polymerization is selective for bioethanol refinery and multi-functional biochar assembly using brittle stalk of corn mutant

Tianqi Li [a,b,1], Hao Peng [a,1], Boyang He [b], Cuiyun Hu [b], Huiyi Zhang [b], Yunong Li [b], Yujing Yang [a,b], Yanting Wang [a,b], Mahmoud M.A. Bakr [b,c], Mengzhou Zhou [a], Liangcai Peng [a,b], Heng Kang [a,b,*]

[a] Key Laboratory of Fermentation Engineering (Ministry of Education), Hubei Key Laboratory of Industrial Microbiology, Biomass & Bioenergy Research Centre, Hubei University of Technology, Wuhan 430068, China
[b] College of Plant Science & Technology, Huazhong Agricultural University, Wuhan 430070, China
[c] Agricultural and Biosystems Engineering Department, Faculty of Agriculture, Damietta University, Damietta 34517, Egypt

ARTICLE INFO

Keywords:
Cellulose nanofibers
Lignocellulose recalcitrance
Biochar adsorption
Electrochemical conductivity
Biochar detoxication

ABSTRACT

As lignocellulose recalcitrance principally restricts for a cost-effective conversion into biofuels and bioproducts, this study re-selected the brittle stalk of corn mutant by *MuDR*-transposon insertion, and detected much reduced cellulose polymerization and crystallinity. Using recyclable CaO chemical for biomass pretreatment, we determined a consistently enhanced enzymatic saccharification of pretreated corn brittle stalk for higher-yield bioethanol conversion. Furthermore, the enzyme-undigestible lignocellulose was treated with two-step thermal-chemical processes via $FeCl_2$ catalysis and KOH activation to generate the biochar with significantly raised adsorption capacities with two industry dyes (methylene blue and Congo red). However, the desirable biochar was attained from one-step KOH treatment with the entire brittle stalk, which was characterized as the highly-porous nanocarbon that is of the largest specific surface area at 1697.34 m^2/g and 2-fold higher dyes adsorption. Notably, this nanocarbon enabled to eliminate the most toxic compounds released from CaO pretreatment and enzymatic hydrolysis, and also showed much improved electrochemical performance with specific capacitance at 205 F/g. Hence, this work has raised a mechanism model to interpret how the recalcitrance-reduced lignocellulose is convertible for high-yield bioethanol and multiple-function biochar with high performance.

1. Introduction

As the most abundant biomass resource, lignocellulose is transformable for sustainable bioethanol and valuable biomaterials to attain carbon neutralization and bioeconomic benefit [1–3]. The bioethanol conversion demands three major strides: initial biomass pretreatment to destruct plant cell walls, sequential enzymatic hydrolysis of pretreated lignocellulose to release fermentable sugars, and final yeast fermentation to produce ethanol [4–6]. Even though lignocellulose is of great potential for industrialization, however, its inherent recalcitrance not only leads to a costly biomass process distasteful for high-yield bioethanol, but it also causes a lowly effective generation of bioproduction with potential secondary pollution to the environment [3,7,8]. It thus endures to explore advanced technology for lignocellulose conversion at cost-effective and green-like style.

Physical and chemical pretreatments can partially break down lignocellulose recalcitrance to enhance biomass enzymatic saccharification for bioethanol production or chemical catalysis for bioproduction, but they principally require extra conditions along with secondary wastes disposition [9]. For examples, acid (H_2SO_4) pretreatments at high temperature and alkali (NaOH) pretreatments at high concentration are mostly implemented for partial hemicelluloses and lignin extraction and lignocellulose feature modification. Therefore, integrating desirable recalcitrance-reduced lignocellulose with green-like pretreatment is increasingly deemed to reduce the cost of biofuels, as well to improve the quality of bioproducts [10–13]. Despite alkaline pretreatment is effective to achieve the goal for plant cell wall depolymerization and destruction, CaO pretreatment has been

* Corresponding author at: Key Laboratory of Fermentation Engineering (Ministry of Education), Hubei Key Laboratory of Industrial Microbiology, Biomass & Bioenergy Research Centre, Hubei University of Technology, Wuhan 430068, China.
E-mail address: hkang@mail.hzau.edu.cn (H. Kang).
[1] These authors contributed equally to this work.

https://doi.org/10.1016/j.ijbiomac.2024.130448
Received 22 December 2023; Received in revised form 20 February 2024; Accepted 23 February 2024
Available online 28 February 2024

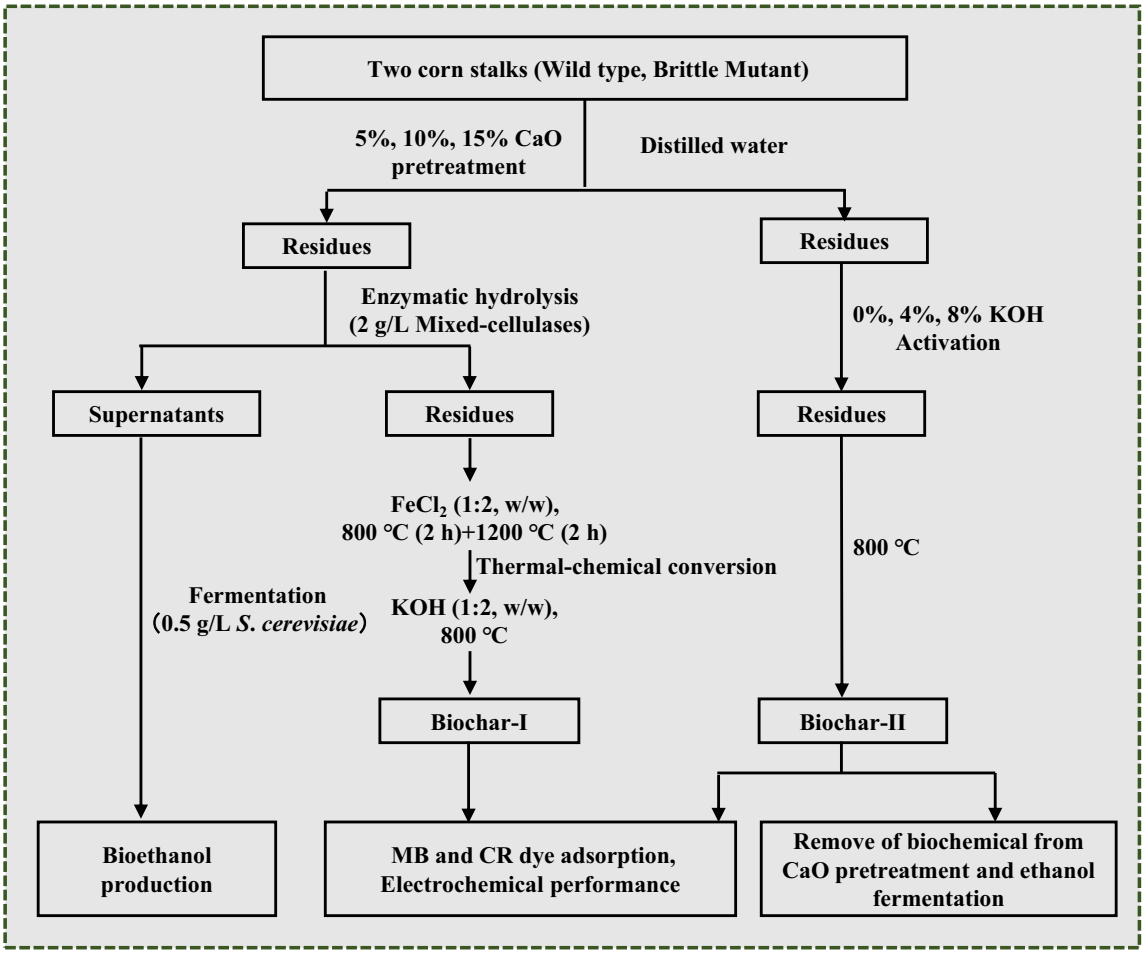

Fig. 1. Flow charts of lignocellulose processes selective for bioethanol conversion and biochar generation to enhance dye and biochemical adsorption and electrochemical performance using corn brittle mutant and its wild type/WT.

particularly applied as a green-like process to improve biomass enzymatic saccharification, due to its mild and simply operation, relatively low cost and recyclable collection [14,15].

Biochar has been extensively exploited for industrial wastes removal and energy storage application, due to its stable structure, large porosity, high specific surface area and excellent electrochemical performance [16–19]. Since lignocellulose contains almost 80 % carbon, it is regarded as one of the most promising precursors for synthesis of desirable carbon materials by advanced thermal-chemical technology [20–24]. Nevertheless, lignocellulose composition and property have a significant influence on biochar quantity and quality. In particular, the oxygen-containing functional groups of cellulose and hemicellulose can be eliminated as H_2O, CO_2 and CO to give micropores of biochar, whereas the plentiful aromatic units of lignin are chemically inert to produce nonporous carbon materials [25]. As biochar is efficient to remove toxic chemical dyes from industry and daily life locations [26–31], the well-quality biochar is also attempted to prepare supercapacitors with high power density, short charge-discharge period and long life [32–34]. Despite thermal-chemical conversion has been well established to generate desirable biochar, chemical activators are increasingly supplied for high-performance carbon production. For examples, the addition of Fe element can form a carburized phase for graphene-like nanosheets during biomass carbonization process [22,35], whereas the K element can join into the carbon structure to improve its porosity [36]. Hence, attention has been paid to conduct optimal thermal-chemical conversion with desirable lignocellulose substrate.

The crop brittle straws have been recently characterized as the recalcitrance-reduced lignocellulose substrates convertible for high-yield biofuel production, but little is yet reported about its application for high-performance biochar. As a widely cultivated crop, corn generates a huge amount of lignocellulose resource every year, and desired corn mutants could particularly improve economic benefits. In this study, we re-planted our recently-identified corn *MuDR*-transposon insertion mutant [37], and determined significantly improved lignocellulose recalcitrant features in the brittle stalk (Fig. 1). By performing CaO pretreatments, this study examined consistently enhanced biomass enzymatic saccharification of corn mutant compared to its wild type/WT, and all remaining enzyme-undigestible residues were employed to generate the biochar with relatively high adsorption with two classic industry dyes (methylene blue/MB and Congo red/CR) and improved electroconductivity. Furthermore, this study performed relatively simply thermal-chemical conversion with the entire brittle stalk to generate the desirable biochar with much improved performance. Notably, this work also employed the desirable biochar to eliminate the most biochemicals remained from CaO pretreatment and final ethanol fermentation (Fig. 1), providing a green-like strategy for reduction of secondary waste release from bioethanol biorefinery. Therefore, this study finally raised a novel model to sort out the mechanism about how the recalcitrance-reduced lignocellulose of brittle stalk was digestible and convertible for high-yield bioethanol and well-performance biochar.

2. Materials and methods

2.1. Collection of corn mature stalks

The corn mutant with brittle stalk phenotype (termed *bk1*) was re-selected from the F_2 seeds of the corn wild type (WT) crossing with *MuDR* transposon *W22::Mu* [37]. The homozygous seeds of WT and mutant were obtained by self-fertilization and their mature stalks were collected in the experimental field of Huazhong Agricultural University from 2020 to 2022. The mature corn stalks were dried at 60 °C, ground through a 60-mesh screen, and stored in a dry container as biomass samples for analyses of cell wall composition, biomass enzymatic hydrolysis and biochar production (Fig. 1).

2.2. Wall polymers extraction and assay

Wall polysaccharide fractionations of mature stalks in corn mutant and WT were accomplished as previously described [38,39]. The soluble sugars were extracted from biomass powder (0.1 g) with potassium phosphate buffer (pH 7.0), the residues were consecutively extracted to remove lipids, starch and pectin by using chloroform-methanol (1:1, v/v), DMSO–water (9:1, v/v), and ammonium oxalate 0.5 % (w/v). The remaining crude residues were extracted with 4 M KOH containing 1.0 mg/mL sodium borohydride for 1 h at 25 °C, and the supernatants were combined as KOH-extractable hemicelluloses fraction. The remaining pellets were applied to detect total pentoses for non-KOH-extractable hemicelluloses fraction. Total hemicelluloses level was calculated by detecting pentoses of the non-KOH-extractable pellets and total hexoses and pentoses in the KOH-extractable fraction. The anthrone/H_2SO_4 and ferric chloride/HCl methods were respectively employed for the analyses of hexoses and pentoses [40]. Total lignin was detected according to the Laboratory Analytical Procedure of the National Renewable Energy Laboratory [41]. All assays were completed in independent triplicates.

2.3. Detection of cellulose features

The crystalline cellulose was extracted from biomass powder (0.1 g) using 5 mL acetic acid-nitric acid-water (8: 1: 2, v/v/v). The degree of polymerization (DP) of cellulose substrate was evaluated by the viscometry method [42], and its crystalline index (CrI) was assessed by the X-ray diffraction [38].

2.4. CaO pretreatments of corn stalks

For CaO pretreatment, biomass powder (0.3 g) was incubated with 6 mL CaO at different concentrations (5 %, 10 %, 15 %, w/w) under 5 % solid loading. After well-mixed, the sample was treated at 50 °C under 150 rpm shaken for 48 h [37]. After centrifugation at 4000 *g*, all residues were collected for enzymatic hydrolysis and biochar conversion as described below. All experiments were fulfilled at independent triplicates.

2.5. Enzymatic saccharification and yeast fermentation

Enzymatic saccharification and yeast fermentation were respectively conducted as previously described [38]. The biomass residues from CaO pretreatment were incubated with 0.16 % (w/v) mixed-cellulases (13.25 FPU g^{-1} cellulases and 8.4 U g^{-1} xylanase from Imperial Jade Biotechnology Co., China) co-supplied with 1 % Tween-80 (v/v). The enzymatic hydrolysis was operated at 50 °C under 150 rpm shaken and the supernatant was saved for yeast fermentation. The activated yeast (Angel yeast Co., ltd., China) was incubated with the enzymatic hydrolysates at 37 °C for 48 h. The fermentation solution was distilled for the determination of ethanol content, and the ethanol was quantified by the $K_2Cr_2O_7$ method as previously described [43].

2.6. Biochar generations from enzyme-undigestible residues and corn stalks

The enzyme-undigestible residues after 15 % CaO pretreatments were well mixed with $FeCl_2{\cdot}4H_2O$ (1:2, w/w), and ground into the powder. The powder sample was loaded into a tube furnace (OTF-1200X-60UV, Kejing Material Technology Co., Ltd., Hefei, China), heated under N_2 at a rate of 5 °C/min up to 800 °C for 2 h, and then up to 1200 °C at the same rate. After the sample was cooled down to 300 °C at a rate of 10 °C/min and further cooled to room temperature, the sample was rinsed with 1 mol/L of HCl aqueous solution for 6 h to remove excess ferric ions. The material was rinsed with deionized water until pH 7.0, washed with ethanol under ultrasound for 2 h in a sonicator, and dried as biocarbon sample. The biocarbon was further mixed with KOH (1:2, w/w), heated at a rate of 5 °C/min up to 800 °C for 3 h, and then cooled down to 300 °C at a rate of 10 °C/min. The residue from KOH treatment was heated at a rate of 5 °C/min up to 800 °C for 3 h, and cooled down to 300 °C at a rate of 10 °C/min. The biochar was stored until in use.

2.7. MB and CR adsorption analysis

MB and CR adsorption were conducted as previously described [10]. MB and CR solution were prepared using ultra-pure water, and about 20 mg biochar and 20 mL MB or CR solution were mixed into 50 mL tube. Adsorption experiments were carried out at 25 °C under 150 rpm shaking for 6 h. After adsorption, the samples were centrifuged at 12,000 *g* for 10 min, and the residual MB and CR in the supernatant were determined by a UV–vis spectrometer at 668 nm and 498 nm, respectively. Using the biochar generated from lignocellulose residues of enzymatic hydrolyses, the initial concentrations of MB and CR solution were 1 g/L and 2 g/L, whereas the biochar generated from full corn stalk applied the initial concentrations of MB and CR at 2 g/L and 10 g/L, respectively. The maximum MB adsorption capacity of biochar was evaluated using monolayer Langmuir adsorption model, and the initial concentrations of MB solution were 0.5, 1, 1.5, 2 and 2.5 g/L.

2.8. Biochemical adsorption assay

Biochar adsorption was performed with the biochemicals released from 15 % Cao pretreatments with corn stalks or final ethanol fermentation. About 40 g/L biochar was incubated with 5 mL biochemicals at 25 °C under 150 rpm shaken for 12 h. After adsorption, the supernatants were passing through 0.22 μm membrane filters to collect the biochemicals. Total organic carbons (TOCs) of the biochemicals were detected by the TOCs analyzer (Multi N/C 3100, Analytik Jena, Germany). All assays were accomplished at independent duplicate.

Total biochemicals and the biochemicals after biochar adsorption were respectively detected by LC-MS/MS (Vanquish, UPLC, Thermo, USA equipped with column Waters HSS T3/100 × 2.1 mm, 1.8 μm and Q Exactive HFX, Thermo, USA), followed with data analysis by Progenesis QI (Waters Corporation, Milford, USA). Total 2756 organics compounds were searched including alkaloids, benzenoids, lipids, organic acids, organoheterocyclic, polyketides, and 1674 compounds were finally identified with a confidence level of over 10 %.

2.9. Detection of electrochemical capacity

The electrochemical properties of biochar were evaluated as previously described [34]. Biochar (0.032 g), Super-P (0.004 g) and PTFE (0.004 g) were mixed with ethanol as the dispersant, and biochar and PTFE were applied as the active material and binder, respectively. The working electrode was prepared by pressing the above mixture onto a current collector, which was nickel foam (1 cm × 1 cm). The test was performed in 6 mol/L of KOH with a three-electrode system, in which a Hg/HgO and a platinum plate were applied as the reference and counter

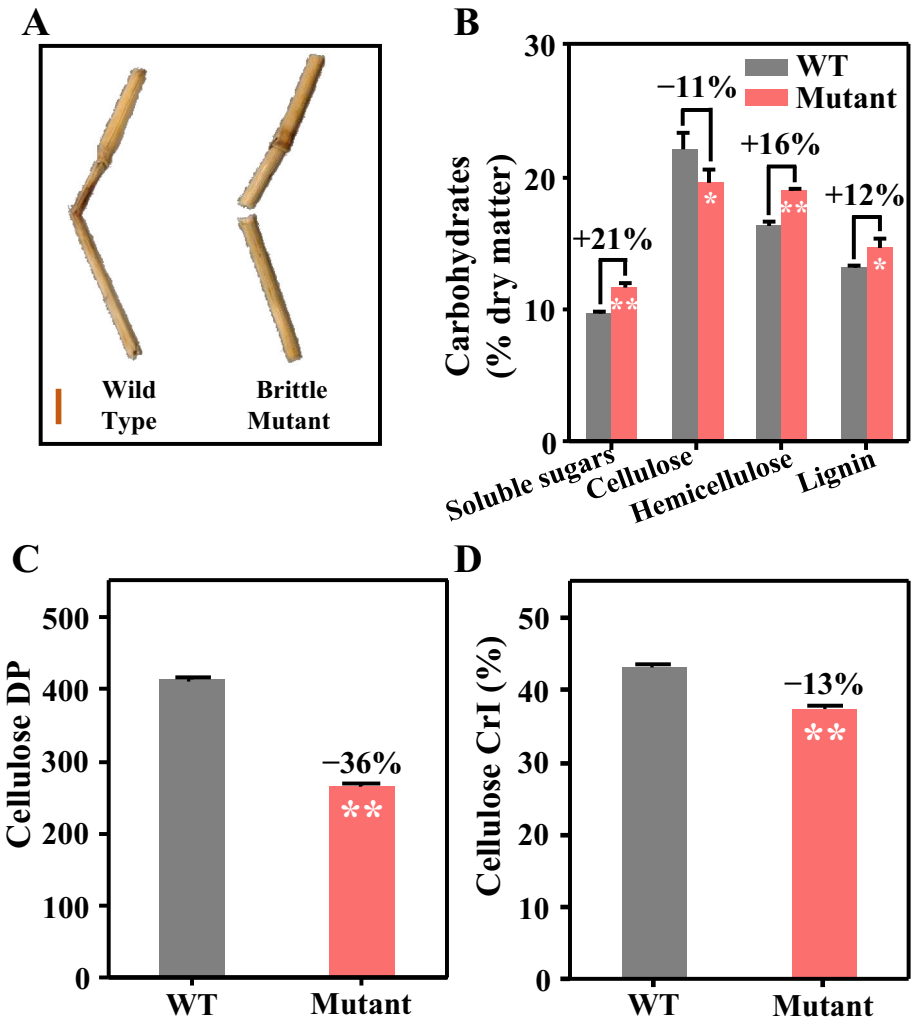

Fig. 2. Detections of lignocellulose composition and cellulose features of mature stalks in corn mutant and WT. (A) A brittle-stalk phenotype of corn mutant under manual bending, bar scaled as 2 cm; (B) Altered cell wall composition (% dry matter); (C) and (D) Significantly reduced degree of polymerization (DP) and crystalline index (CrI) of cellulose microfibrils; * And ** as significant differences between the mutant and WT by Student's *t*-test at $p < 0.05$ and 0.01 levels ($n = 3$); Data as means ± SD (n = 3), and the increased (+) or decreased (−) percentage was calculated by subtraction of the mutant and WT values divided by WT.

electrodes, respectively.

Cyclic voltammetry (CV) and galvanostatic charge–discharge (GCD) were performed on a CHI660E electrochemical workstation to evaluate the electrochemical performance. The CV was completed at scan rates of 50 mV/s, and GCD was conducted at current densities from 0.5 to 10 A/g. The specific capacitance (C, F/g) based on GCD test was calculated according to the Eq. (1):

$$C = I \times \Delta t / (m \times \Delta V)$$

in this formula, I, Δt and ΔV represent for the discharging current (A), discharging time (s) and discharging voltage (V) excluding the IR drop during the discharging process; m (g) is the mass of active material in the working electrode [44].

2.10. Physical and chemical characterization of biochar

The biochar was scanned under high resolution transmission electron microscope (HRTEM, JEOL JEM F200, Tokyo, Japan) and Raman spectrum (Thermo Scientific DXR, Waltham, MA, USA) as described [22]. The elements and binding energy of biochar were detected by X-ray photoelectron spectroscopy (XPS, Thermo Scientific K-Alpha, Waltham, MA, USA) as described [45]. Specific surface area, pore diameter and pore volume of biochar were analyzed by Automated Surface Area and Porosity Analyzer (Micromeritics ASAP 2460, Norcross, GA, USA) as described [46].

2.11. Statistical analysis

Analyses of variance (ANOVA), regression coefficients and Spearman's rank correlation coefficient were respectively attained using Superior Performance Software System (SPSS version 16.0, Inc., Chicago, IL). Pair-wise comparisons were accomplished between two measurements by Student's *t*-test. The line graph, histogram, and regression analysis for the best fit curve were plotted using Origin 8.5 software (Microcal Software, Northampton, MA). The average values were calculated from the original independent triplicate measurements for these analyses.

3. Results and discussion

3.1. Recalcitrance-reduced lignocellulose regeneratable in corn mutant

In this study, we re-selected the corn mutant as previously reported by *MuDR*-transposon insertion [37], and observed a brittle-stalk phenotype under manual bending (Fig. 1; Fig. 2A). By collecting mature brittle stalk of the corn mutant, this study determined

Table 1
Biomass saccharification and bioethanol production in corn mutant and WT after CaO pretreatments.

Samples	CaO pretreatment (w/w)	Hexose yield (% cellulose)	Ethanol yield (% cellulose)	Total ethanol yield in theory (% dry matter)
WT	5 %	45.62 ± 0.26	15.62 ± 0.81	12.91 ± 0.04
Mutant		46.86 ± 0.39** (3 %)[#]	19.27 ± 0.22** (23 %)	14.66 ± 0.23** (14 %)
WT	10 %	54.86 ± 1.81	24.48 ± 0.31	15.99 ± 0.03
Mutant		60.88 ± 0.58** (11 %)	27.33 ± 0.35** (12 %)	16.77 ± 0.24** (5 %)
WT	15 %	82.12 ± 0.61	36.85 ± 0.28	22.31 ± 0.05
Mutant		93.90 ± 1.64** (14 %)	40.61 ± 0.44** (10 %)	24.34 ± 0.21** (9 %)

* And ** as significant differences between the mutant and WT by Student's *t*-test at $p < 0.05$ and 0.01 ($n = 3$), and data as means ± SD; [#]Percentage of increased rate by subtraction between the mutant and WT values divided by the WT.

significantly reduced cellulose level by 11 % and raised hemicellulose and lignin contents by 16 % and 12 % at $p < 0.01$ and 0.05 levels ($n = 3$), compared to its WT (Fig. 2B), which was different from the previous report about much less cellulose level and similar contents of other wall polymers [37]. Meanwhile, we examined total soluble sugars level increased by 21 % in the brittle mutant (Table S1), but it is raised by 65 % in the previous one, which should be mainly due to less reduced cellulose and significantly increased hemicellulose in this study. Furthermore, the brittle mutant showed more decreased cellulose DP value by 36 % than the previously-reported one by 17 % (Fig. 2C), which should be partially due to significantly raised hemicellulose level examined in this work [40,47,48]. As cellulose DP value and hemicellulose level are highly correlated with cellulose CrI [47,49], this study also detected significantly reduced cellulose CrI value in the brittle mutant (Fig. 2D), which should be accounting for more reduction of lignocellulose recalcitrance examined in this study [4,42]. Because the brittle mutant is identified from a genetically-stable homozygous line, the relatively-altered cell wall composition, cellulose features (DP, CrI) and soluble sugars level may be due to varied conditions for plant growth, stalk harvest stage and climate in this study, which was consistent with the previous findings about the distinct geographic locations and ecological conditions that affect plant cell wall compositions [50–52]. On the other hand, this study may also indicate a strategy for collection of recalcitrance-reduced lignocellulose resources by growing desirable crop mutants under optimal field management and ecological condition.

3.2. Consistently enhanced biomass saccharification for bioethanol production

Using our previously-established approach [37,38,53], this study examined biomass saccharification by measuring hexose yields (% cellulose) released from enzymatic hydrolyses after 5 %, 10 %, 15 % CaO pretreatments with mature stalks in corn mutant and WT (Fig. 1). As a result, the brittle mutant showed consistently raised hexoses yields (% cellulose) than those of the WT at $p < 0.01$ levels ($n = 3$) under all CaO pretreatments (Table 1). In particular, about 94 % cellulose of the corn mutant could be digested upon 15 % CaO pretreatment, whereas 82 % cellulose degradation occurred in the WT. Even though the corn mutant contained significantly higher lignin level than that of WT (Fig. 2B), which has been characterized as a major barrier against enzyme access and loading [54–56], much more reduced cellulose features (DP, CrI) should improve its lignocellulose recalcitrance for consistently enhanced biomass enzymatic saccharification examined. Consequently, this study performed a classic yeast fermentation with hexoses released from enzymatic hydrolysis, and also detected constantly raised

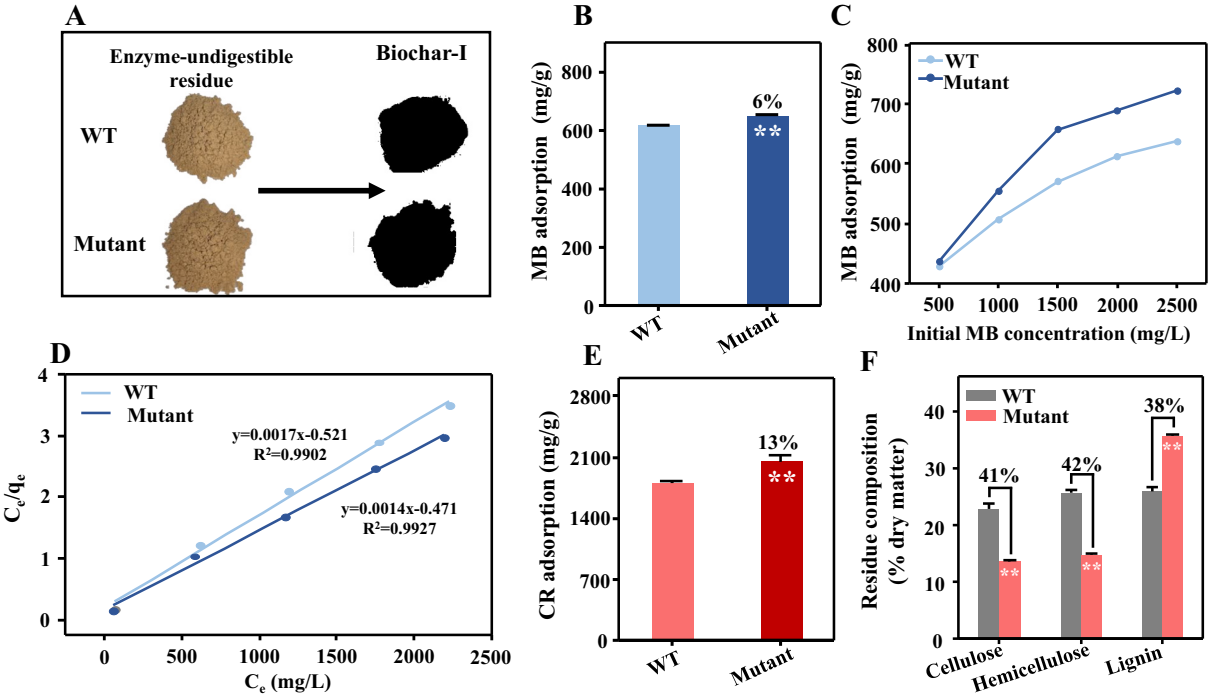

Fig. 3. Characterization of the biochar-I generated from lignocellulose residues of enzymatic hydrolyses after 15 %CaO pretreatments with mature stalks in corn mutant and WT. (A) Schematic of the thermal-chemical conversion; (B) Biochar adsorption with methylene blue/MB; (C) MB adsorption capacity under different initial concentrations; (D) Langmuir adsorption isotherm model for maximum MB adsorption; (E) Biochar adsorption with Congo red/CR; (F) Wall polymer compositions of enzymatic residues; ** As significant difference between the corn mutant and WT by Student's *t*-test at $p < 0.01$ ($n = 3$) with the increased/decreased (−) percentage of the corn mutant relative to the WT, and data as means ± SD ($n = 3$).

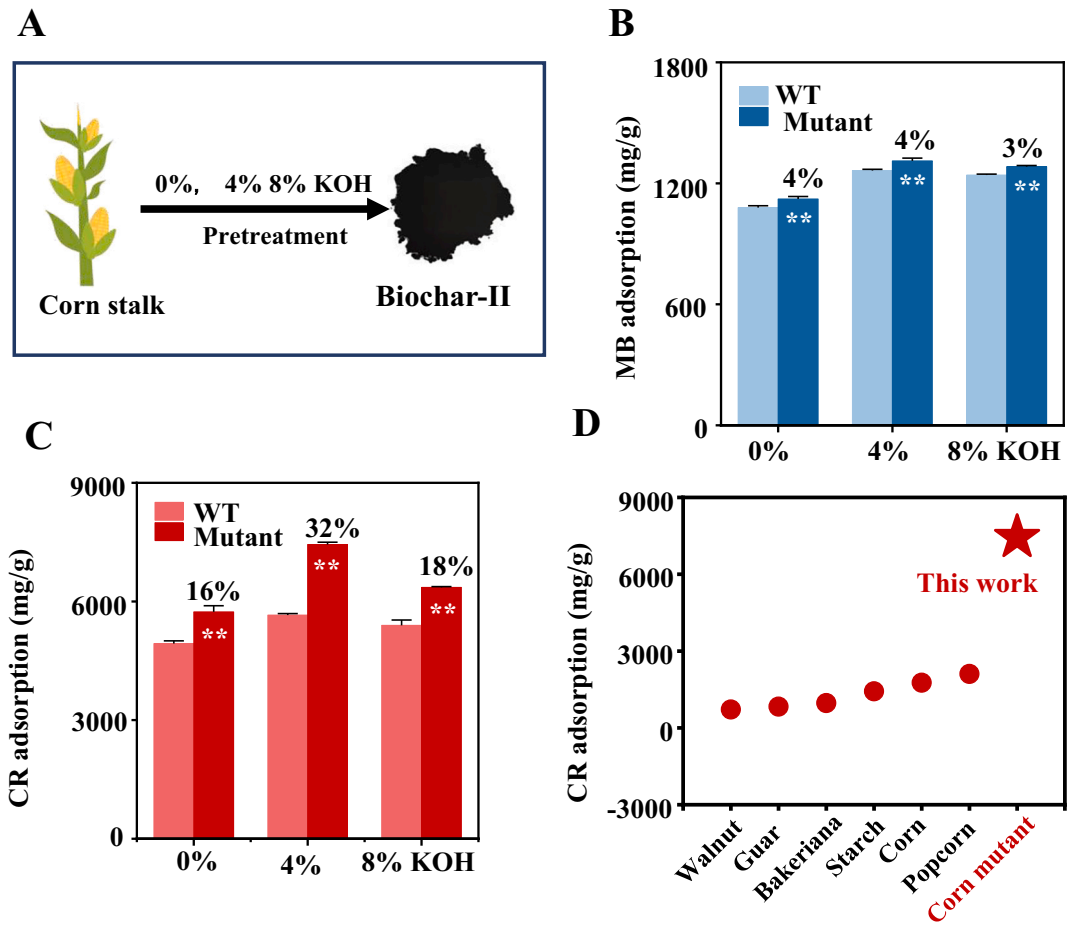

Fig. 4. Characterization of the biochar-II generated from entire mature stalks of corn mutant and WT. (A) Schematic of the thermal-chemical conversion after KOH pretreatments; (B, C) biochar adsorption with MB and CR; (D) comparison of CR adsorptions among biochar samples as previously generated from other biomass resources; ** As significant difference between the corn mutant and WT by Student's *t*-test at $p < 0.01$ ($n = 3$) with the increased/decreased (–) percentage of the corn mutant relative to the WT, and data as means ± SD ($n = 3$).

bioethanol yields (% cellulose) by 10 %–23 % at $p < 0.01$ level ($n = 3$) in the mutant compared to the WT (Table 1). Moreover, we evaluated total bioethanol yields (% dry matter) in theory from engineered-yeast co-fermentation with total hexoses and xylose of soluble sugars and enzymatic hydrates. As a comparison, the corn mutant remained more raised bioethanol yields than those of the WT, mainly due to its significantly increased soluble sugars and hemicellulose levels. As lignocellulose recalcitrance is consistently reduced in the corn mutant, it remains to explore its potential utilization for valuable bioproduction.

3.3. Biochar generation from enzyme-undigestible residues for dyes adsorption

To avoid any remaining biomass residues release into the environment, we collected all residues obtained from enzymatic hydrolyses of 15 % CaO-pretreated corn stalks in mutant and WT, and performed a thermal-chemical conversion co-activated with $FeCl_2{\cdot}4H_2O$ and KOH chemicals to generate biochar termed as biochar-I (Fig. 1; Fig. 3A). By means of our recently-established approaches [10,45,57], this study tested biochar adsorption with two major industry dyes: methylene blue (MB), a common cationic organic dye, and Congo red (CR), a typical anionic organic dye. As a result, the biochar sample generated from corn mutant showed significantly higher adsorption capacities with MB at $p < 0.01$ level ($n = 3$), compared to the WT (Fig. 3B). By supplying MB at a series of concentrations for batch experiments, the typical Langmuir models were established with extremely high R^2 values for both biochar samples of corn mutant and WT, but the mutant sample remained consistently higher MB adsorptions than those of the WT examined (Fig. 3C–D). Meanwhile, the corn mutant sample was examined with significantly higher CR adsorption than that of the WT by 13 % (Fig. 3E), and both mutant and WT samples were of greatly higher CR adsorption capacities than those of the MB up to 3 folds, probably due to the biochar containing the Fe^{2+} and K^+ that are active for CR interaction [33,58,59]. To understand the MB and CR adsorption distinctive in the corn mutant and WT, we examined the composition of enzyme-undigestible residues after 15 % CaO pretreatments with corn stalks (Fig. 3F). Because the corn mutant showed significantly raised biomass enzymatic saccharification as described above (Table 1), its remaining residue consisted of much reduced cellulose and hemicellulose levels than those of WT by 41 % and 42 %, leading to the lignin content raised by 38 %. It thus suggests that the residue rich at lignin should be one of major factors accounting for the biochar with high MB and CR adsorption as previously reported [10,45,57].

3.4. Maximum dye adsorption by biochar generated from entire brittle stalk

Given that the biochar of corn mutant was of significantly higher CR and MB adsorptions than those of the WT as described above, their adsorption capacities remained relatively low, compared to the previously-reported ones [60–62]. Hence, this study employed entire brittle stalks to generate new biochar termed as biochar-II by performing relatively simply KOH-activated pyrolysis (Fig. 1; Fig. 4A). In general, this study detected the highest CR and MB adsorption capacities with the

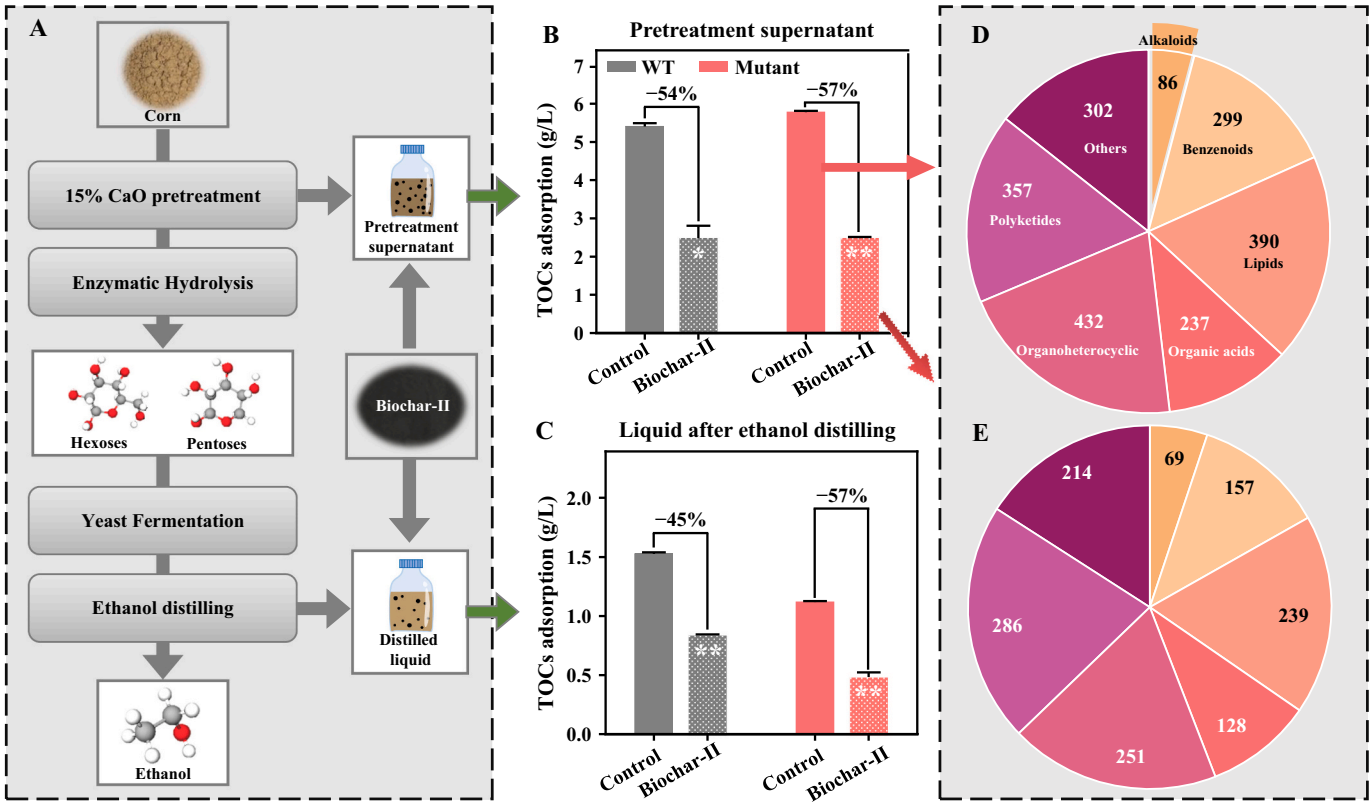

Fig. 5. Characterization of biochar-II adsorption with total organic carbons (TOCs) released from either 15 % CaO pretreatments or yeast fermentation in corn mutant and WT. (A) Schematic of two TOCs resources from ethanol refinery; (B, C) biochar-II adsorptions with two TOCs resources, control as original TOCs without biochar adsorption; (D) molecular amounts of all major types of chemicals detected by LC-MS analysis in the supernatant of 15 % CaO pretreatment with mutant stalk; (E) molecular amounts of the chemicals that were adsorbed by biochar-II; * And ** as significant differences between the mutant and WT by Student's *t*-test at $p < 0.05$ or 0.01 level; Data as means ± SD.

biochar samples generated from 4 % KOH activation with both corn mutant and WT, compared with the control (without KOH) and 8 % KOH treatment (Fig. 4B–C). In particular, all biochar samples of corn mutant remained consistently higher CR and MB adsorption capacities than those of the WT, and the CR adsorption capacities were increased by 16 %–32 % in the mutant samples. Furthermore, the MB and CR adsorption capacities were respectively raised by 2- and 3.6 folds in the biochar-II generated from entire brittle stalk of corn mutant, compared to the biochar-I samples generated from enzyme-undigestible residues as described above (Fig. 3). Notably, as a comparison with the biochar samples as previously generated from other major biomass resources, the biochar-II of corn mutant was of the highest CR adsorption capacity with raised rates by 3.5–8.9 folds (Fig. 4D; Table S2). The results thus indicated that the entire brittle stalk of corn mutant could be applied to generate the optimal biochar for maximum dye adsorption from simply thermal-chemical conversion.

However, as those two types of biochar showed distinct adsorption capacities with chemical dyes, this study has provided the comparable samples to explore biochar adsorption mechanisms for its specific application by characterization of their physical and chemical properties (Fig. S1). These may also help to sort out distinct biochar assembly by performing correlation analyses between lignocellulose features and thermal-chemical conductive conditions, which should be an interesting study in the future.

3.5. *Effective exclusion of toxic biochemicals released from ethanol biorefinery*

As toxic biochemicals are unavoidably released from cellulosic ethanol biorefinery [27,63,64], this study detected biochar adsorption with the liquids remained from biomass pretreatment and final ethanol fermentation in corn mutant and WT samples (Fig. 1; Fig. 5A). Using the biochar-II sample of corn mutant, we examined that about 54 % and 57 % of total organic carbon (TOC) were respectively removed from the supernatants of 15 % CaO pretreatments with the mature stalks of corn mutant and WT (Fig. 5B). Despite that TOCs were much less released in the liquids of final ethanol fermentation, this study also tested 45 % and 57 % TOCs removal with the biochar-II in the corn mutant and WT samples (Fig. 5C), indicating that the biochar-II was effective to remove almost half of TOCs released from the ethanol biorefinery performed in this study. On the other hand, the biochar of mutant sample could extract relatively more TOCs than those of the WT, in particular for the liquids of ethanol fermentation. It suggests that toxic TOCs were less produced in the mutant sample, which should be another factor accounting for significant higher bioethanol conversion achieved in the mutant.

Moreover, we applied LC-MS/MS to detect the composition of TOCs that were adsorbed with biochar-II using the liquid released from CaO pretreatment of corn mutant (Fig. 5D). In general, the biochar-II could adsorb diverse biochemicals such as alkaloids, benzenoids, lipid, organic acids, organoheterocyclic and polyketides. In particular, about 53 %–80 % components could be completely removed by the biochar-II among all six types of chemicals examined (Fig. 6E), which confirmed that the biochar-II could mostly eliminate the toxic compounds released from bioethanol biorefinery. On the other hands, the remaining TOCs unadsorbed with biochar-II should be mainly derived from the pentoses and hexoses released from CaO pretreatment performed in this study.

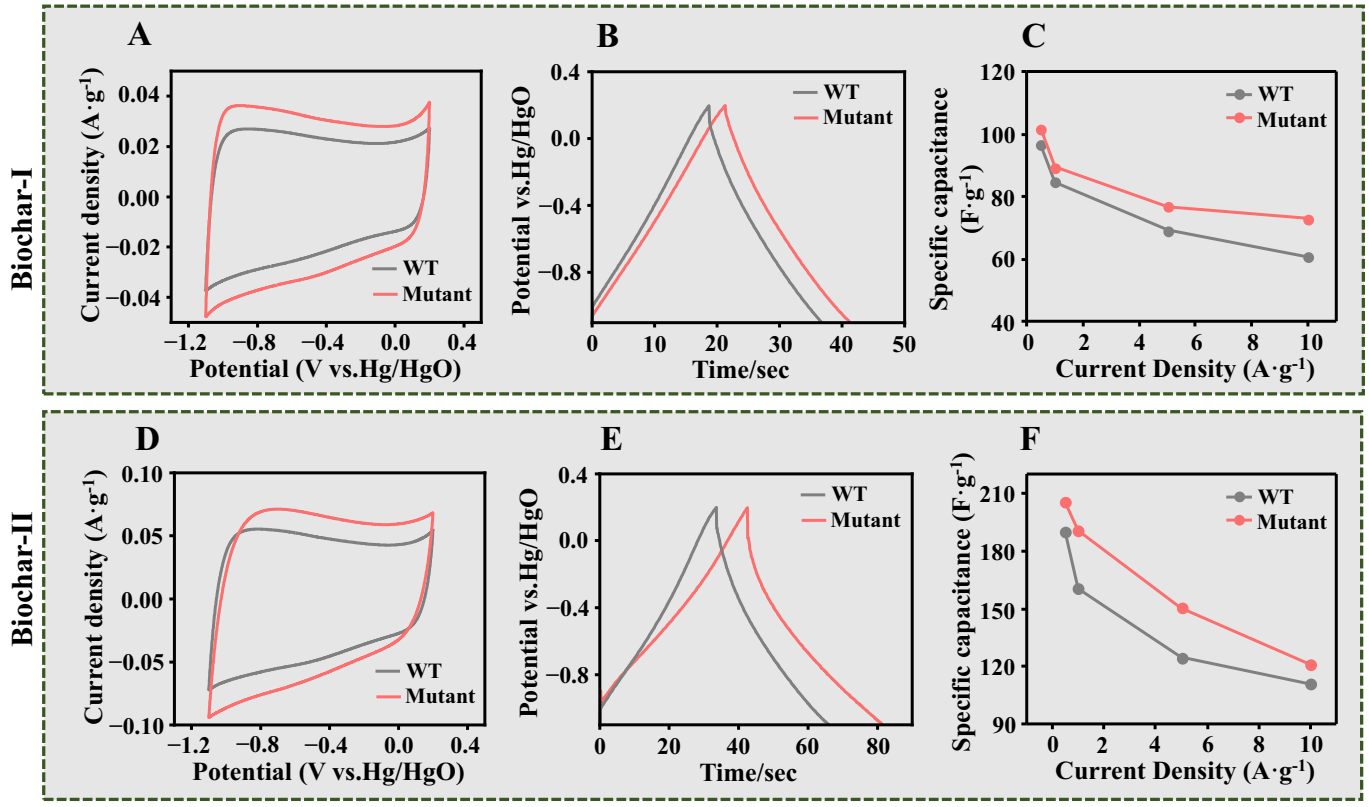

Fig. 6. Enhanced electrochemical performances using biochar-I generated from enzymatic residues or biochar-II from entire mature stalks of corn mutant and WT. (A, D) Cyclic voltammetry curves at 50 mV·s^{-1}; (B, E) Galvanostatic charge-discharge curves at 5 A·g^{-1}; (C, F) Specific capacitance calculated by galvanostatic charge-discharge at different current densities.

3.6. 3.6 Improved electrochemical performance

To find out other function of two types of biochar samples (I, II) generated above, this study tested their electrochemical performances for supercapacitor (Fig. 1; Fig. 6). In terms of the electronic transport of biochar-I sample, the cyclic voltammograms (CVs) were recorded at scan rates from 5 to 150 mV/s to detect the power capability. The obtained stable current response up to 50 mV/s showed that the biochar sample of corn mutant was of higher current density than that of the WT (Fig. 6A). While galvanostatic charge-discharge (GCD) tests were conducted, a typical inverted "V" shape was observed in both mutant and WT samples, suggesting a classic capacitive response and fast charge transfer [58,65–67] (Fig. 6B). However, the mutant sample remained a much longer discharging time for the highest specific capacitance in the electrolyte systems at different current densities from 0.5 A/g to 10 A/g, compared to the WT. With respect to the capacitance values calculated from the GCD curves at different current densities, the mutant sample exhibited consistently higher specific capacitances than those of the WT (Fig. 6C), thereby confirming a consistently improved electrochemical performance for supercapacitor in the mutant.

Furthermore, this study detected the electrochemical performances of the biochar-II samples (Fig. 6D–E). Constantly, the biochar-II samples of corn mutant were of higher electrochemical conductivity and specific capacitances than those of the WT, being similar to the findings examined in the biochar-I. However, the biochar-II samples showed the specific capacitances raised up to 2 folds, compared to the biochar-I ones. Taken together, therefore, the brittle stalk of corn mutant could provide options selective either to achieve higher bioethanol production or to

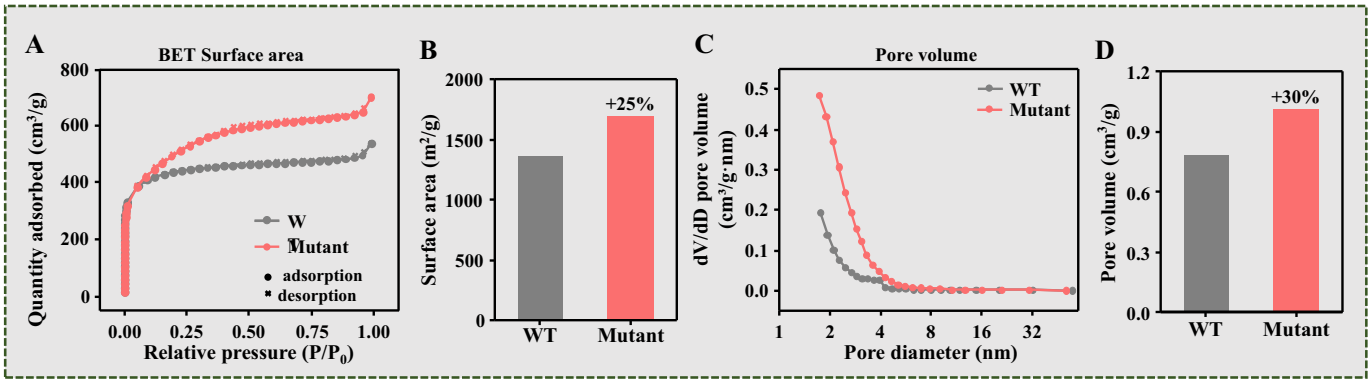

Fig. 7. Increased BET surface area and pore volume of the biochar-II generated from entire mature stalks of corn mutant and WT after 4 % KOH pretreatment. (A) Nitrogen adsorption/desorption isotherm; (B) Surface area; (C) Pore size distribution; (D) Pore volume.

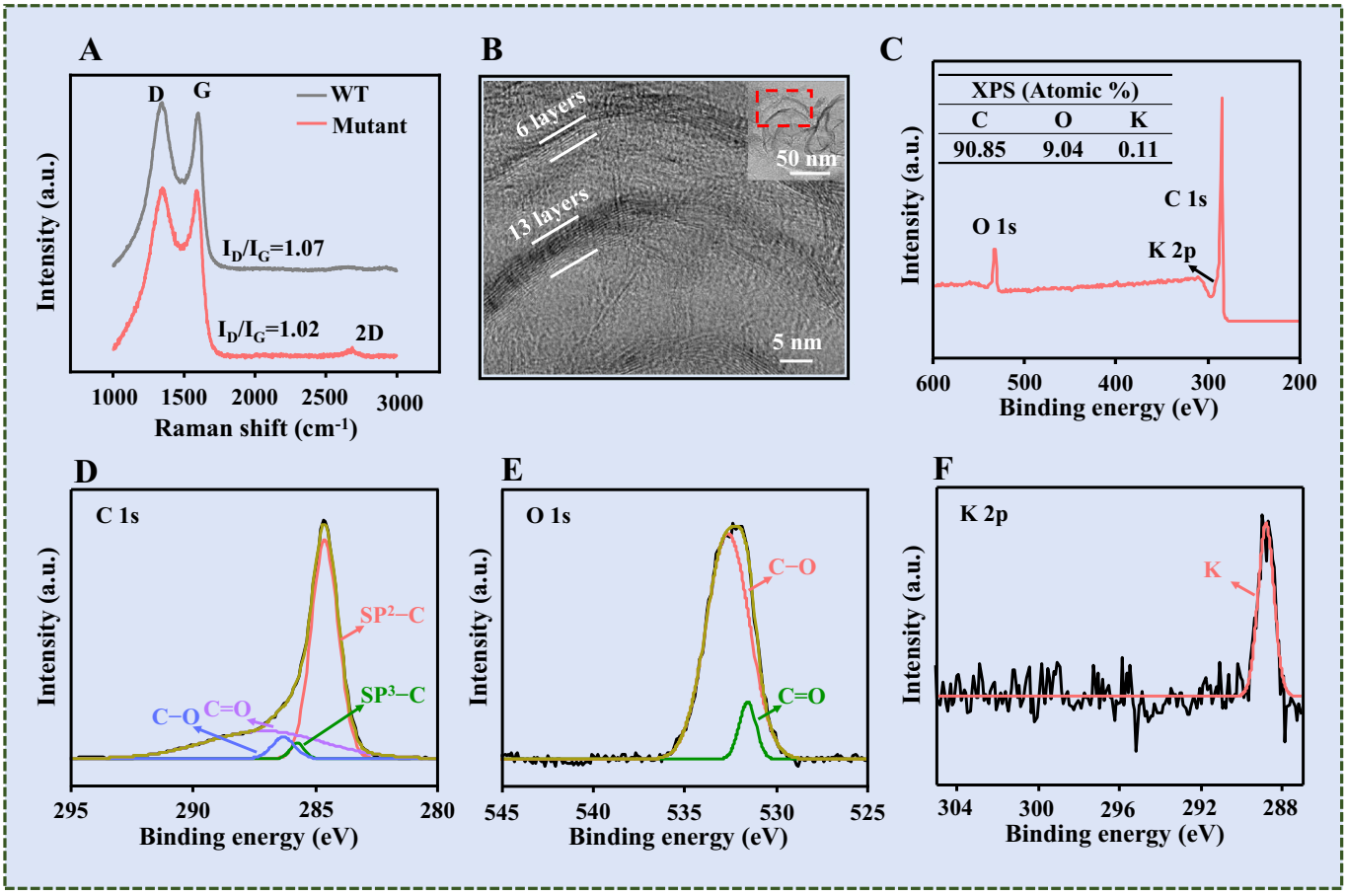

Fig. 8. Characterization of the biochar-II generated from the mature entire stalks of corn mutant and WT after 4 % KOH pretreatment. (A) Raman spectra profiles for typical G and 2D peaks as graphene-like carbon; (B) nanocarbon observation as 6- and 13-layer graphene under high resolution transmission electron microscopy in the biochar sample of corn mutant; (C) XPS spectra profile of the biochar sample of corn mutant; (D–F) high-resolution XPS spectrum at C1s region (D), O1s region (E) and K2p region (F) in the biochar sample of corn mutant.

generate distinct biochar for enhanced dye and biochemical adsorption and electrochemical performance.

3.7. Increased porosity of graphene-like biochar

As the biochar-II sample was of much improved dye and biochemical adsorption and electrochemical performance in the corn mutant, this study conducted a classic BET assay by N_2 absorption (Fig. 7). As a comparison, the biochar-II of corn mutant exhibited consistently larger BET areas than those of the WT (Fig. 7A). For example, the total surface area of mutant sample was calculated at 1697.34 m^2/g, but the WT only reached to 1363.07 m^2/g (Fig. 7B). Meanwhile, a typical adsorption isotherm was observed to be accountable for the presence of micro-pores in the mutant sample (Fig. 7C), and its pore volume under <4 nm diameter was raised by 30 %, compared to the WT (Fig. 7D). Hence, the increases of both surface area and pore volumes of biochar-II in the mutant should be the major cause for remarkably improved dye and biochemical adsorption and electrochemical performances examined above.

Meanwhile, Raman scanning was implemented with the biochar-II samples (Fig. 8), and a typical G-peak (~1580 cm^{-1}) was observed (Fig. 8A), revealing that the graphene-like carbon could be obtained by 4 % KOH activated thermal-chemical conversion with entire corn stalks. However, only mutant sample displayed 2D peak, and it also had a relatively lower I_D: I_G ratio than that of the WT sample, suggesting that the biochar of mutant sample should be of relatively higher graphitic intensity and reduced defect density [68–71]. Under high resolution transmission electron microscopy, we observed that the mutant sample consisted of 6-13 graphene layers as nanocarbon (Fig. 8B). Based on XPS assay, the nanocarbon of mutant sample contained 90.85 % carbon (C) and 9.04 % oxygen (O) with 0.11 % K (Fig. 8C). Four typical peaks were further identified to correspond for sp^2-bonded carbon (284.6 eV), sp^3-C (285.8 eV), C—O (286.3 eV), C═O (287.1 eV) [69,72] (Fig. 8D). Accordingly, the O1s spectrum was of two peaks corresponding to C═O (531.6 eV) and C—O (532.7 eV) [71] (Fig. 8E), but the peak at 288.8 eV was examined to correspond to K (Fig. 8F), due to KOH activation. Therefore, the results confirmed that the desirable graphene-like nanocarbon could be achieved by coupling KOH pretreatment and thermal-chemical conversion with entire brittle stalk of corn mutant.

3.8. Mechanisms of high bioethanol production and desirable biochar generation

To understand how the brittle stalk of corn mutant could produce high-yield bioethanol and high-performance biochar, we raised a mechanism model to link all major findings achieved in this study (Fig. 9). By re-selecting *MuDR* transposon insertion corn mutant, this study initially collected recalcitrance-improved lignocellulose substrates accountable by reduced cellulose CrI and DP values. Because cellulose CrI and DP have been well characterized as two crucial negative factors on lignocellulose enzymatic hydrolyses in the most bioenergy crops examined [30,73–76], it is simply understandable for biomass saccharification and bioethanol conversion raised in the corn mutant, compared to the WT. As the corn mutant was of the mostly

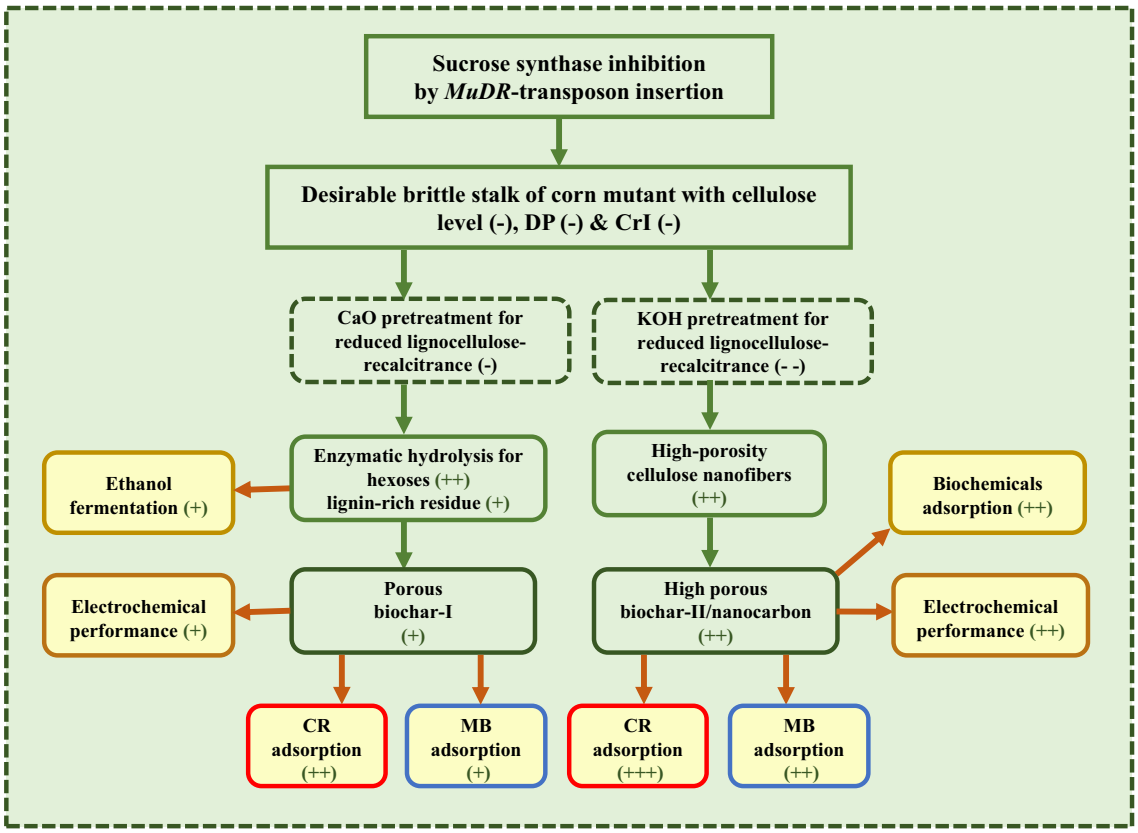

Fig. 9. A mechanism model to elucidate how cellulose recalcitrance is improved in brittle stalk of corn mutant, which is favor for bioethanol conversion and biochar generation selective for enhanced dyes and chemicals elimination and electrochemical performance. (+) And (−) as increased and decreased factors/parameters, respectively.

enhanced cellulose enzymatic hydrolysis, its remaining residue is rich at lignin, which should be the major factor for the biochar-I with improved dye adsorption and electrochemical performance [22]. However, it remains to further explore how the biochar-I of mutant residue is of better electrochemical performance than that of the WT in the future.

With respect to the desirable biochar-II that was of even more improved performances (dye and biochemical adsorption, electrochemical conductivity), we assumed that it is mainly due to highly-porous nanocarbon generation in the corn mutant (Fig. 10). As length-reduced cellulose nanofibers could be generated by genetic engineering and alkali pretreatment for double-reduction of lignocellulose recalcitrance accountable by low-DP cellulose microfibrils assembly [12], we also presumed that the high-density cellulose nanofiber assembly should occur in the mutant, which may cause the porous nanocarbon formation [22]. In addition, as Fe and K elements could respectively activate to form a graphene-like and highly-porous nanocarbon during biomass carbonization process [22,35], it remains to further improve quality and quantity of the nanocarbons by integrating desirable corn mutants with optimal biomass processes in the future.

4. Conclusions

By collecting the desirable brittle stalk of corn mutant with *MuDR* transposon insertion for sucrose synthase inhibition, this study determined recalcitrance-improved lignocellulose substrate accountable by significantly reduced cellulose CrI and DP values, leading to consistently enhanced biomass enzymatic saccharification and bioethanol conversion. The remaining lignin-rich residue was further applied to generate the porous biochar effective for dyes adsorption and supercapacitor performance. Notably, highly-porous nanocarbon was produced with the largest specific surface area by performing one-step thermal-chemical conversion with entire brittle stalk, which was detected with the upgraded MB adsorption by 2 folds or the highest CR adsorption or the better electrochemical performance. In addition, this study detected that the nanocarbon could eliminate the most toxic compounds released from CaO pretreatment and enzymatic hydrolysis.

Hence, this study has raised a mechanism model to highlight how the desirable lignocellulose of corn mutant is digestible for bioethanol production and convertible for highly-porous nanocarbon generation with multiple improved performances, providing a green-like strategy for full utilization of crop straws.

CRediT authorship contribution statement

Tianqi Li: Writing – review & editing, Writing – original draft, Validation, Supervision, Software, Formal analysis, Data curation. **Hao Peng:** Writing – review & editing, Writing – original draft, Validation, Investigation, Formal analysis, Data curation. **Boyang He:** Writing – review & editing, Writing – original draft, Validation, Supervision, Resources, Formal analysis, Data curation. **Cuiyun Hu:** Validation, Supervision, Methodology, Investigation. **Huiyi Zhang:** Validation, Supervision, Methodology, Investigation, Data curation. **Yunong Li:** Validation, Supervision, Methodology, Investigation, Data curation. **Yujing Yang:** Validation, Supervision, Methodology, Investigation, Data curation. **Yanting Wang:** Validation, Supervision, Software, Resources, Methodology, Investigation, Funding acquisition, Data curation, Conceptualization. **Mahmoud M.A. Bakr:** Validation, Supervision, Investigation. **Mengzhou Zhou:** Validation, Supervision, Project administration, Methodology, Funding acquisition. **Liangcai Peng:** Writing – review & editing, Writing – original draft, Validation, Supervision, Software, Resources, Project administration, Methodology, Investigation, Funding acquisition, Formal analysis, Data curation,

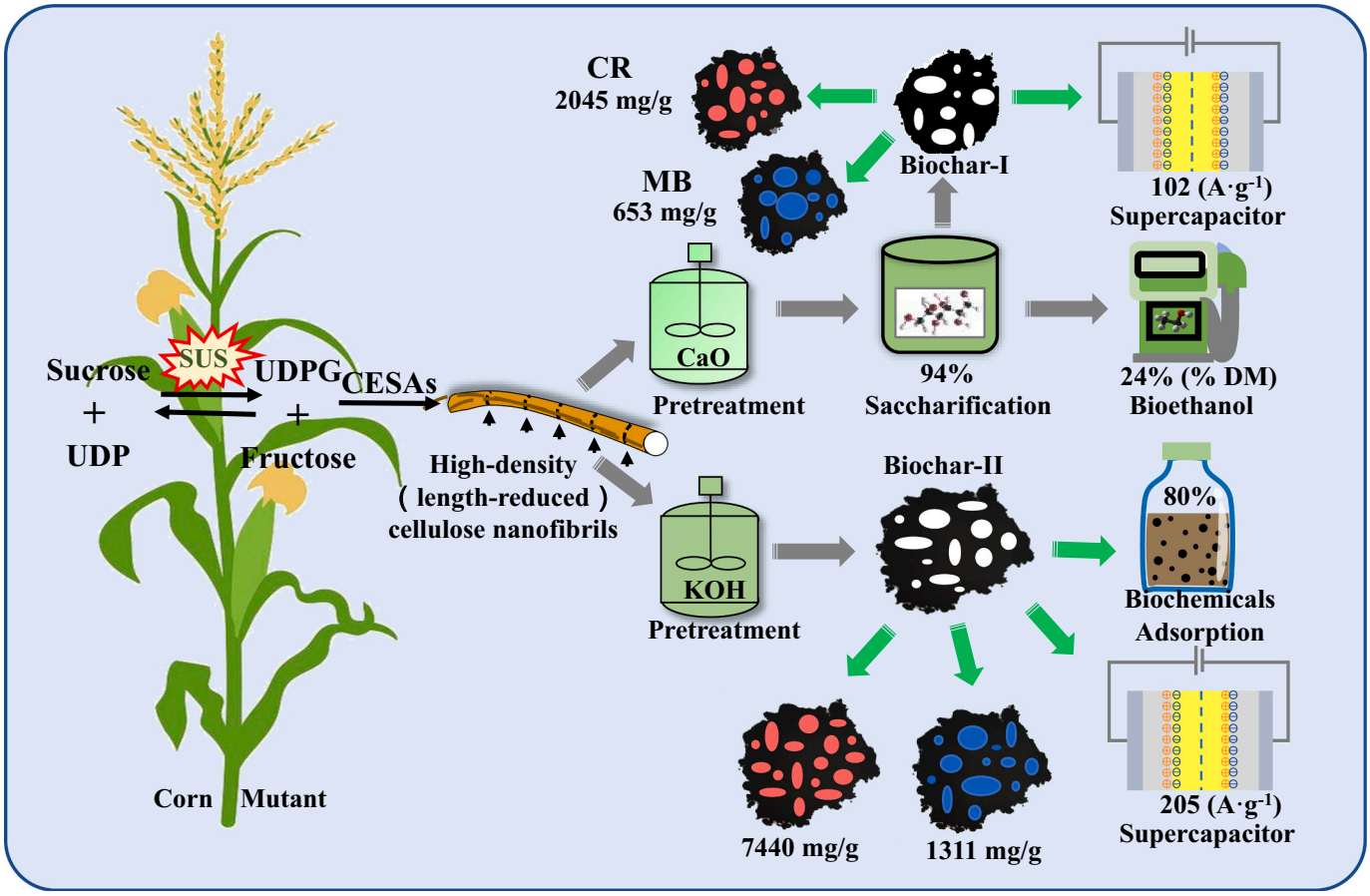

Fig. 10. A graphic model links all major findings and novelty achieved in this study.

Conceptualization. **Heng Kang:** Writing – review & editing, Writing – original draft, Validation, Supervision, Software, Resources, Methodology, Funding acquisition, Formal analysis, Data curation, Conceptualization.

Declaration of competing interest

The authors have no conflicts of interest to declare.

Acknowledgments

This work was in part supported by the National Natural Science Foundation of China (32070095, 32101701, 32170268), National 111 Project of Ministry of Education of China (BP0820035, D17009), and Initiative Grant of Hubei University of Technology for High-level Talents (GCC20230001).

Appendix A. Supplementary data

Supplementary data to this article can be found online at https://doi.org/10.1016/j.ijbiomac.2024.130448.

References

[1] Y.M. Wang, P. Liu, G.F. Zhang, Q.M. Yang, J. Lu, T. Xia, L.C. Peng, Y.T. Wang, Cascading of engineered bioenergy plants and fungi sustainable for low-cost bioethanol and high-value biomaterials under green-like biomass processing, Renew. Sustain. Energy Rev. 137 (2021) 110586, https://doi.org/10.1016/j.rser.2020.110586.

[2] B. Sharma, C. Larroche, C.-G. Dussap, Comprehensive assessment of 2G bioethanol production, Bioresour. Technol. 313 (2020), https://doi.org/10.1016/j.biortech.2020.123630.

[3] Y.T. Wang, C.F. Fan, H.Z. Hu, Y. Li, D. Sun, Y.M. Wang, L.C. Peng, Genetic modification of plant cell walls to enhance biomass yield and biofuel production in bioenergy crops, Biotechnol. Adv. 34 (5) (2016) 997–1017, https://doi.org/10.1016/j.biotechadv.2016.06.001.

[4] H.R. Gao, Y.T. Wang, Q.M. Yang, H. Peng, Y.Q. Li, D. Zhan, H.T. Wei, H.W. Lu, M. M.A. Bakr, M.M. Ei-Sheekh, Z. Qi, L.C. Peng, X.C. Lin, Combined steam explosion and optimized green-liquor pretreatments are effective for complete saccharification to maximize bioethanol production by reducing lignocellulose recalcitrance in one-year-old bamboo, Renew. Energ. 175 (2021) 1069–1079, https://doi.org/10.1016/j.renene.2021.05.016.

[5] R.O.M.A. de Souza, L.S.M. Miranda, R. Luque, Bio (chemo) technological strategies for biomass conversion into bioethanol and key carboxylic acids, Green Chem. 16 (5) (2014) 2386–2405, https://doi.org/10.1039/C3GC41885E.

[6] I.A. Ndubuisi, C.O. Amadi, T.N. Nwagu, Y. Murata, J.C. Ogbonna, Non-conventional yeast strains: unexploited resources for effective commercialization of second generation bioethanol, Biotechnol. Adv. 63 (2023) 108100, https://doi.org/10.1016/j.biotechadv.2023.108100.

[7] P. Liu, A. Li, Y.M. Wang, Q.M. Cai, H.Z. Yu, Y.Q. Li, H. Peng, Q. Li, Y.T. Wang, X. Y. Wei, R. Zhang, Y.Y. Tu, T. Xia, L.C. Peng, Distinct *Miscanthus* lignocellulose improves fungus secreting cellulases and xylanases for consistently enhanced biomass saccharification of diverse bioenergy crops, Renew. Energ. 174 (2021) 799–809, https://doi.org/10.1016/j.renene.2021.04.107.

[8] E.M. Rubin, Genomics of cellulosic biofuels, Nature 454 (7206) (2008) 841–845, https://doi.org/10.1038/nature07190.

[9] Q.J. Chen, Y.L. Zhao, Q.H. Xie, C.Y. Liang, Z.Y. Zong, Polyethyleneimine grafted starch nanocrystals as a novel biosorbent for efficient removal of methyl blue dye, Carbohydr. Polym. 273 (2021), https://doi.org/10.1016/j.carbpol.2021.118579.

[10] Z. Hu, Q. Li, Y.Y. Chen, T.Q. Li, Y.M. Wang, R. Zhang, H. Peng, H.L. Wang, Y. T. Wang, J.F. Tang, M. Nauman Aftab, L.C. Peng, Intermittent ultrasound retains cellulases unlock for enhanced cellulosic ethanol with high-porosity biochar for dye adsorption using desirable rice mutant straw, Bioresour. Technol. 369 (2023) 128437, https://doi.org/10.1016/j.biortech.2022.128437.

[11] H. Peng, W.Y. Zhao, J.Y. Liu, P. Liu, H.Z. Yu, J. Deng, Q.M. Yang, R. Zhang, Z. Hu, S.L. Liu, D. Sun, L.C. Peng, Y.T. Wang, Distinct cellulose nanofibrils generated for improved Pickering emulsions and lignocellulose-degradation enzyme secretion coupled with high bioethanol production in natural rice mutants, Green Chem. 24 (7) (2022) 2975–2987, https://doi.org/10.1039/D1GC04447H.

[12] R. Zhang, Z. Hu, H. Peng, P. Liu, Y.M. Wang, J.Y. Li, J. Lu, Y.T. Wang, T. Xia, L. C. Peng, High density cellulose nanofibril assembly leads to upgraded enzymatic and chemical catalysis of fermentable sugars, cellulose nanocrystals and cellulase

production by precisely engineering cellulose synthase complexes, Green Chem. 25 (3) (2023) 1096–1106, https://doi.org/10.1039/D2GC03744K.
[13] X.X. Zhou, J. Zhao, M.Z. Chen, S.P. Wu, G.Y. Zhao, S. Xu, Effects of hydration parameters on chemical properties of biocrudes based on machine learning and experiments, Bioresour. Technol. 350 (2022), https://doi.org/10.1016/j.biortech.2022.126923.
[14] L.W. He, C. Wang, H.H. Shi, W. Zhou, Q. Zhang, X.Y. Chen, Combination of steam explosion pretreatment and anaerobic alkalization treatment to improve enzymatic hydrolysis of *Hippophae rhamnoides*, Bioresour. Technol. 289 (2019) 121693, https://doi.org/10.1016/j.biortech.2019.121693.
[15] L.L. Cheng, L.Q. Wang, L.Y. Wei, Y. Wu, A. Alam, C.B. Xu, Y.T. Wang, Y.Y. Tu, L. C. Peng, T. Xia, Combined mild chemical pretreatments for complete cadmium release and cellulosic ethanol co-production distinctive in wheat mutant straw, Green Chem. 21 (13) (2019) 3693–3700, https://doi.org/10.1039/C9GC00686A.
[16] A. Dutta, J. Mahanta, T. Banerjee, Supercapacitors in the light of solid waste and energy management: a review, Adv. Sustain. Syst. 4 (12) (2020) 2000182, https://doi.org/10.1002/adsu.202000182.
[17] M. Gao, W.-K. Wang, Y.-M. Zheng, Q.-B. Zhao, H.-Q. Yu, Hierarchically porous biochar for supercapacitor and electrochemical H_2O_2 production, Chem. Eng. J. 402 (2020) 126171, https://doi.org/10.1016/j.cej.2020.126171.
[18] X.X. Zhou, T.B. Moghaddam, M.Z. Chen, S.P. Wu, Y. Zhang, X.R. Zhang, S. Adhikari, X. Zhang, Effects of pyrolysis parameters on physicochemical properties of biochar and bio-oil and application in asphalt, Sci. Total Environ. 780 (2021) 146448, https://doi.org/10.1016/j.scitotenv.2021.146448.
[19] K.Z. Qian, A. Kumar, H.L. Zhang, D. Bellmer, R. Huhnke, Recent advances in utilization of biochar, Renew. Sustain. Energy Rev. 42 (2015) 1055–1064, https://doi.org/10.1016/j.rser.2014.10.074.
[20] M. Borghei, J. Lehtonen, L. Liu, O.J. Rojas, Advanced biomass-derived electrocatalysts for the oxygen reduction reaction, Adv. Mater. 30 (24) (2017), https://doi.org/10.1002/adma.201703691.
[21] L.M.N. Lakmini, A.D.K. Deshan, H.D. Pham, W. Doherty, D. Rackemann, D. P. Dubal, L. Moghaddam, High carbon utilization: 5-(chloromethyl) furfural (CMF) production from rice by-products and transformation of CMF residues into Li-ion energy storage systems, J. Clean. Prod. 375 (2022) 134082, https://doi.org/10.1016/j.jclepro.2022.134082.
[22] J.Y. Liu, X. Zhang, H. Peng, T.Q. Li, P. Liu, H.R. Gao, Y.T. Wang, J.F. Tang, Q. Li, Z. Qi, L.C. Peng, T. Xia, Full-chain $FeCl_3$ catalyzation is sufficient to boost cellulase secretion and cellulosic ethanol along with valorized supercapacitor and biosorbent using desirable corn stalk, Molecules (2023), https://doi.org/10.3390/molecules28052060.
[23] V. Pavlenko, S. Khosravi H, S. Żółtowska, A.B. Haruna, M. Zahid, Z. Mansurov, Z. Supiyeva, A. Galal, K.I. Ozoemena, Q. Abbas, T. Jesionowski, A comprehensive review of template-assisted porous carbons: modern preparation methods and advanced applications, Mater. Sci. Eng. R. Rep. 149 (2022) 100682, https://doi.org/10.1016/j.mser.2022.100682.
[24] G.Y. Zhang, X. Liu, L. Wang, H.G. Fu, Recent advances of biomass derived carbon-based materials for efficient electrochemical energy devices, J. Mater. Chem. A 10 (17) (2022) 9277–9307, https://doi.org/10.1039/D2TA01442D.
[25] Y.L. Li, H. Yu, L.N. Liu, H.B. Yu, Application of co-pyrolysis biochar for the adsorption and immobilization of heavy metals in contaminated environmental substrates, J. Hazard. Mater. 420 (2021) 126655, https://doi.org/10.1016/j.jhazmat.2021.126655.
[26] N. Saman, J.-W. Tan, S.S. Mohtar, H.L. Kong, J.W.P. Lye, K. Johari, H. Hassan, H. Mat, Selective biosorption of aurum(III) from aqueous solution using oil palm trunk (OPT) biosorbents: equilibrium, kinetic and mechanism analyses, Biochem. Eng. J. 136 (2018) 78–87, https://doi.org/10.1016/j.bej.2018.05.004.
[27] S.M. Shaheen, N.K. Niazi, N.E.E. Hassan, I. Bibi, H. Wang, Daniel C.W. Tsang, Y. S. Ok, N. Bolan, J. Rinklebe, Wood-based biochar for the removal of potentially toxic elements in water and wastewater: a critical review, Int. Mater. Rev. 64 (4) (2018) 216–247, https://doi.org/10.1080/09506608.2018.1473096.
[28] K. Yadav, S.R. Latelwar, D. Datta, B. Jana, Efficient removal of MB dye using litchi leaves powder adsorbent: isotherm and kinetic studies, J. Indian Chem. Soc. 100 (4) (2023) 100974, https://doi.org/10.1016/j.jics.2023.100974.
[29] S.J. Ye, M. Yan, X.F. Tan, J. Liang, G.M. Zeng, H.P. Wu, B. Song, C.Y. Zhou, Y. Yang, H. Wang, Facile assembled biochar-based nanocomposite with improved graphitization for efficient photocatalytic activity driven by visible light, Appl Catal B 250 (2019) 78–88, https://doi.org/10.1016/j.apcatb.2019.03.004.
[30] X.X. Zhou, L. Shi, T.B. Moghaddam, M.Z. Chen, S.P. Wu, X.Z. Yuan, Adsorption mechanism of polycyclic aromatic hydrocarbons using wood waste-derived biochar, J. Hazard. Mater. 425 (2022) 128003, https://doi.org/10.1016/j.jhazmat.2021.128003.
[31] X.X. Zhou, T.B. Moghaddam, M.Z. Chen, S.P. Wu, S. Adhikari, Biochar removes volatile organic compounds generated from asphalt, Sci. Total Environ. 745 (2020), https://doi.org/10.1016/j.scitotenv.2020.141096.
[32] A. González, E. Goikolea, J.A. Barrena, R. Mysyk, Review on supercapacitors: technologies and materials, Renew. Sustain. Energy Rev. 58 (2016) 1189–1206, https://doi.org/10.1016/j.rser.2015.12.249.
[33] F. Jiang, Y.H. Zhu, Z. Liu, X. Zhang, W. Ma, H.T. Wu, X.H. Huang, Q. Zhang, Novel synthesis route for the preparation of mesoporous nitrogen-doped carbons from forestry wastes for supercapacitors, Surf. Interfaces 24 (2021), https://doi.org/10.1016/j.surfin.2021.101132.
[34] P. Wang, G. Zhang, M.-Y. Li, Y.-X. Yin, J.-Y. Li, G. Li, W.-P. Wang, W. Peng, F.-F. Cao, Y.-G. Guo, Porous carbon for high-energy density symmetrical supercapacitor and lithium-ion hybrid electrochemical capacitors, Chem. Eng. J. 375 (2019) 122020, https://doi.org/10.1016/j.cej.2019.122020.
[35] L. Sun, C. Tian, M. Li, X. Meng, L. Wang, R. Wang, J. Yin, H. Fu, From coconut shell to porous graphene-like nanosheets for high-power supercapacitors, J. Mater. Chem. A 1 (21) (2013) 6462–6470, https://doi.org/10.1039/C3TA10897J.
[36] Q. Chen, X.F. Tan, Y.G. Liu, S.B. Liu, M.F. Li, Y.L. Gu, P. Zhang, S.J. Ye, Z.Z. Yang, Y.Y. Yang, Biomass-derived porous graphitic carbon materials for energy and environmental applications, J. Mater. Chem. A 8 (12) (2020) 5773–5811, https://doi.org/10.1039/C9TA11618D.
[37] L.M. Wu, S.Q. Feng, J. Deng, B. Yu, Y.M. Wang, B.Y. He, H. Peng, Q. Li, R.F. Hu, L. C. Peng, Altered carbon assimilation and cellulose accessibility to maximize bioethanol yield under low-cost biomass processing in corn brittle stalk, Green Chem. 21 (16) (2019) 4388–4399, https://doi.org/10.1039/C9GC01237K.
[38] Y. Li, P. Liu, J.F. Huang, R. Zhang, Z. Hu, S.Q. Feng, Y.T. Wang, L.Q. Wang, T. Xia, L.C. Peng, Mild chemical pretreatments are sufficient for bioethanol production in transgenic rice straws overproducing glucosidase, Green Chem. 20 (9) (2018) 2047–2056, https://doi.org/10.1039/C8GC00694F.
[39] L.C. Peng, C.H. Hocart, J.W. Redmond, R.E. Williamson, Fractionation of carbohydrates in *Arabidopsis* root cell walls shows that three radial swelling loci are specifically involved in cellulose production, Planta 211 (3) (2000) 406–414, https://doi.org/10.1007/s004250000301.
[40] N. Xu, W. Zhang, S.F. Ren, F. Liu, C.Q. Zhao, H.F. Liao, Z.D. Xu, J.F. Huang, Q. Li, Y.Y. Tu, B. Yu, Y.T. Wang, J.X. Jiang, J.P. Qin, L.C. Peng, Hemicelluloses negatively affect lignocellulose crystallinity for high biomass digestibility under NaOH and H_2SO_4 pretreatments in *Miscanthus*, Biotechnol. Biofuels 5 (1) (2012) 58, https://doi.org/10.1186/1754-6834-5-58.
[41] Z.Y. Zhang, I.M. O'Hara, W.O.S. Doherty, Pretreatment of sugarcane bagasse by acid-catalysed process in aqueous ionic liquid solutions, Bioresour. Technol. 120 (2012) 149–156, https://doi.org/10.1016/j.biortech.2012.06.035.
[42] W. Zhang, Z.L. Yi, J.F. Huang, F.C. Li, B. Hao, M. Li, S.F. Hong, Y.Z. Lv, W. Sun, A. Ragauskas, F. Hu, J.H. Peng, L.C. Peng, Three lignocellulose features that distinctively affect biomass enzymatic digestibility under NaOH and H_2SO_4 pretreatments in *Miscanthus*, Bioresour. Technol. 130 (2013) 30–37, https://doi.org/10.1016/j.biortech.2012.12.029.
[43] J. Littlewood, L. Wang, C. Turnbull, R.J. Murphy, Techno-economic potential of bioethanol from bamboo in China, Biotechnol. Biofuels 6 (1) (2013) 173, https://doi.org/10.1186/1754-6834-6-173.
[44] K.O. Oyedotun, F. Barzegar, A.A. Mirghni, A.A. Khaleed, T.M. Masikhwa, N. Manyala, Examination of high-porosity activated carbon obtained from dehydration of white sugar for electrochemical capacitor applications, ACS Sustain. Chem. Eng. 7 (1) (2019) 537–546, https://doi.org/10.1021/acssuschemeng.8b04080.
[45] H. Yu, M. Hu, Z. Hu, F. Liu, H.Z. Yu, Q.M. Yang, H.R. Gao, C.B. Xu, M.L. Wang, G. F. Zhang, Y. Wang, T. Xia, L.C. Peng, Y.T. Wang, Insights into pectin dominated enhancements for elimination of toxic Cd and dye coupled with ethanol production in desirable lignocelluloses, Carbohydr. Polym. 286 (2022) 119298, https://doi.org/10.1016/j.carbpol.2022.119298.
[46] R. Zhang, Z. Hu, Y.T. Wang, H.Z. Hu, F.C. Li, M. Li, A. Ragauskas, T. Xia, H.Y. Han, J.F. Tang, H.Z. Yu, B.Q. Xu, L.C. Peng, Single-molecular insights into the breakpoint of cellulose nanofibers assembly during saccharification, Nat. Commun. 14 (1) (2023) 1100, https://doi.org/10.1038/s41467-023-36856-8.
[47] F.C. Li, G.S. Xie, J.F. Huang, R. Zhang, Y. Li, M.M. Zhang, Y.T. Wang, A. Li, X.K. Li, T. Xia, C.C. Qu, F. Hu, A.J. Ragauskas, L.C. Peng, OsCESA9 conserved-site mutation leads to largely enhanced plant lodging resistance and biomass enzymatic saccharification by reducing cellulose DP and crystallinity in rice, Plant Biotechnol. J. 15 (9) (2017) 1093–1104, https://doi.org/10.1111/pbi.12700.
[48] L.M. Wu, M. Li, J.F. Huang, H. Zhang, W.H. Zou, S.W. Hu, Y. Li, C.F. Fan, R. Zhang, H.C. Jing, L.C. Peng, S.Q. Feng, A near infrared spectroscopic assay for stalk soluble sugars, bagasse enzymatic saccharification and wall polymers in sweet sorghum, Bioresour. Technol. 177 (2015) 118–124, https://doi.org/10.1016/j.biortech.2014.11.073.
[49] M. Hu, H. Yu, Y. Li, A. Li, Q.M. Cai, P. Liu, Y.Y. Tu, Y.T. Wang, R.F. Hu, B. Hao, L. C. Peng, T. Xia, Distinct polymer extraction and cellulose DP reduction for complete cellulose hydrolysis under mild chemical pretreatments in sugarcane, Carbohydr. Polym. 202 (2018) 434–443, https://doi.org/10.1016/j.carbpol.2018.08.039.
[50] H.Z. Hu, R. Zhang, Z.S. Tao, X.K. Li, Y.Y. Li, J.F. Huang, X.X. Li, X. Han, S.Q. Feng, G.M. Zhang, L.C. Peng, Cellulose synthase mutants distinctively affect cell growth and cell wall integrity for plant biomass production in *Arabidopsis*, Plant Cell Physiol. 59 (6) (2018) 1144–1157, https://doi.org/10.1093/pcp/pcy050.
[51] S. Rebello, A.N. Anoopkumar, E.M. Aneesh, R. Sindhu, P. Binod, A. Pandey, Sustainability and life cycle assessments of lignocellulosic and algal pretreatments, Bioresour. Technol. 301 (2020) 122678, https://doi.org/10.1016/j.biortech.2019.122678.
[52] Z.R. Li, C.Q. Zhao, Y. Zha, C. Wan, S.L. Si, F. Liu, R. Zhang, F.C. Li, B. Yu, Z.L. Yi, N. Xu, L.C. Peng, Q. Li, The minor wall-networks between monolignols and interlinked-phenolics predominantly affect biomass enzymatic digestibility in *Miscanthus*, PloS One 9 (8) (2014) e105115, https://doi.org/10.1371/journal.pone.0105115.
[53] S.J. Song, F.W. Ma, G. Wu, D. Ma, W.D. Geng, J.F. Wan, Facile self-templating large scale preparation of biomass-derived 3D hierarchical porous carbon for advanced supercapacitors, J. Mater. Chem. A 3 (35) (2015) 18154–18162, https://doi.org/10.1039/C5TA04721H.
[54] J. Deng, T.Y. Xiong, H.Y. Wang, A.M. Zheng, Y. Wang, Effects of cellulose, hemicellulose, and lignin on the structure and morphology of porous carbons, ACS Sustain. Chem. Eng. 4 (7) (2016) 3750–3756, https://doi.org/10.1021/acssuschemeng.6b00388.

[55] W.X. Jin, L. Chen, M. Hu, D. Sun, A. Li, Y. Li, Z. Hu, S.G. Zhou, Y.Y. Tu, T. Xia, Y. T. Wang, G.S. Xie, Y.B. Li, B.W. Bai, L.C. Peng, Tween-80 is effective for enhancing steam-exploded biomass enzymatic saccharification and ethanol production by specifically lessening cellulase absorption with lignin in common reed, Appl. Energ. 175 (2016) 82–90, https://doi.org/10.1016/j.apenergy.2016.04.104.

[56] J.L. Xu, J.J. Cheng, R.R. Sharma-Shivappa, J.C. Burns, Lime pretreatment of switchgrass at mild temperatures for ethanol production, Bioresour. Technol. 101 (8) (2010) 2900–2903, https://doi.org/10.1016/j.biortech.2009.12.015.

[57] L. Jiang, Y.Y. Wen, Z.J. Zhu, X.F. Liu, W. Shao, A double cross-linked strategy to construct graphene aerogels with highly efficient methylene blue adsorption performance, Chemosphere 265 (2021), https://doi.org/10.1016/j.chemosphere.2020.129169.

[58] A.C. Arampatzidou, E.A. Deliyanni, Comparison of activation media and pyrolysis temperature for activated carbons development by pyrolysis of potato peels for effective adsorption of endocrine disruptor bisphenol-A, J. Colloid Interface Sci. 466 (2016) 101–112, https://doi.org/10.1016/j.jcis.2015.12.003.

[59] F. Rahmawati, A.F. Ridassepri, A.T. Chairunnisa, K. Wijayanta, J. Nakabayashi, T. Miyazaki Miyawaki, Carbon from bagasse activated with water vapor and its adsorption performance for methylene blue, Appl. Sci. (2021), https://doi.org/10.3390/app11020678.

[60] F.J. Chacón, M.L. Cayuela, H. Cederlund, M.A. Sánchez-Monedero, Overcoming biochar limitations to remediate pentachlorophenol in soil by modifying its electrochemical properties, J. Hazard. Mater. 426 (2022), https://doi.org/10.1016/j.jhazmat.2021.127805.

[61] B. Song, X.W. Cao, W.R. Gao, S. Aziz, S. Gao, C.-H. Lam, R.C. Lin, Preparation of nano-biochar from conventional biorefineries for high-value applications, Renew. Sustain. Energy Rev. 157 (2022) 112057, https://doi.org/10.1016/j.rser.2021.112057.

[62] H.N. Tran, F. Tomul, N. Thi Hoang Ha, D.T. Nguyen, E.C. Lima, G.T. Le, C.-T. Chang, V. Masindi, S.H. Woo, Innovative spherical biochar for pharmaceutical removal from water: insight into adsorption mechanism, J. Hazard. Mater. 394 (2020) 122255, https://doi.org/10.1016/j.jhazmat.2020.122255.

[63] M.K. Monjed, B. Achour, G.D. Robson, J.K. Pittman, Improved saccharification of *Chlorella vulgaris* biomass by fungal secreted enzymes for bioethanol production, Algal Res. 58 (2021) 102402, https://doi.org/10.1016/j.algal.2021.102402.

[64] H.N. Nassar, W.I.M. El-azab, N.S. El-Gendy, Sustainable ecofriendly recruitment of bioethanol fermentation lignocellulosic spent waste biomass for the safe reuse and discharge of petroleum production produced water via biosorption and solid biofuel production, J. Hazard. Mater. 422 (2022) 126845, https://doi.org/10.1016/j.jhazmat.2021.126845.

[65] J.B. Kim, S.H. Koo, I.H. Kim, J.T. Kim, J.G. Kim, B. Jayaraman, J. Lim, S.O. Kim, Characteristic dual-domain composite structure of reduced graphene oxide and its application to higher specific capacitance, Chem. Eng. J. 446 (2022) 137390, https://doi.org/10.1016/j.cej.2022.137390.

[66] H. Xie, Q.Q. Zhao, Z.R. Zhou, Y.M. Wu, H.C. Wang, H. Xu, Correction: efficient removal of Cd(II) and cu(II) from aqueous solution by magnesium chloride-modified *Lentinula edodes*, RSC Adv. 5 (44) (2015) 35097, https://doi.org/10.1039/C5RA90038G.

[67] K.X. Zou, Y.F. Deng, W.J. Wu, S.W. Zhang, G.H. Chen, A novel eutectic solvent precursor for efficiently preparing N-doped hierarchically porous carbon nanosheets with unique surface functional groups and micropores towards dual-carbon lithium-ion capacitors, J. Mater. Chem. A 9 (23) (2021) 13631–13641, https://doi.org/10.1039/D1TA03071J.

[68] C. Zhang, D.Y. Qin, Y. Zhou, F.Z. Qin, H. Wang, W.J. Wang, Y. Yang, G.M. Zeng, Dual optimization approach to Mo single atom dispersed g-C3N4 photocatalyst: morphology and defect evolution, Appl Catal B 303 (2022) 120904, https://doi.org/10.1016/j.apcatb.2021.120904.

[69] X. Kong, Y.F. Zhu, H.W. Lei, C.X. Wang, Y.F. Zhao, E.G. Huo, X.N. Lin, Q.F. Zhang, M. Qian, W. Mateo, R.G. Zou, Z. Fang, R. Ruan, Synthesis of graphene-like carbon from biomass pyrolysis and its applications, Chem. Eng. J. 399 (2020) 125808, https://doi.org/10.1016/j.cej.2020.125808.

[70] A.C. Ferrari, J.C. Meyer, V. Scardaci, C. Casiraghi, M. Lazzeri, F. Mauri, S. Piscanec, D. Jiang, K.S. Novoselov, S. Roth, A.K. Geim, Raman spectrum of graphene and graphene layers, Phys. Rev. Lett. 97 (18) (2006) 187401, https://doi.org/10.1103/PhysRevLett.97.187401.

[71] Z.C. Chen, S.Y. Liao, L.Y. Ge, P.N. Amaniampong, Y.G. Min, C.H. Wang, K.X. Li, J. M. Lee, Reduced graphene oxide with controllably intimate bifunctionality for the catalytic transformation of fructose into 2,5-diformylfuran in biphasic solvent systems, Chem. Eng. J. 379 (2020) 122284, https://doi.org/10.1016/j.cej.2019.122284.

[72] Y. Wang, Z.M. Rong, Y. Wang, T. Wang, Q.Q. Du, Y. Wang, J.P. Qu, Graphene-based metal/acid bifunctional catalyst for the conversion of levulinic acid to γ-valerolactone, ACS Sustain. Chem. Eng. 5 (2) (2017) 1538–1548, https://doi.org/10.1021/acssuschemeng.6b02244.

[73] M. Madadi, Y.M. Wang, C.B. Xu, P. Liu, Y.T. Wang, T. Xia, Y.Y. Tu, X.C. Lin, B. Song, X.E. Yang, W.B. Zhu, D.Q. Duanmu, S.W. Tang, L.C. Peng, Using *Amaranthus* green proteins as universal biosurfactant and biosorbent for effective enzymatic degradation of diverse lignocellulose residues and efficient multiple trace metals remediation of farming lands, J. Hazard. Mater. 406 (2021) 124727, https://doi.org/10.1016/j.jhazmat.2020.124727.

[74] Y.T. Wang, J.F. Huang, Y. Li, K. Xiong, Y.M. Wang, F.C. Li, M.Y. Liu, Z.L. Wu, Y. Y. Tu, L.C. Peng, Ammonium oxalate-extractable uronic acids positively affect biomass enzymatic digestibility by reducing lignocellulose crystallinity in *Miscanthus*, Bioresour. Technol. 196 (2015) 391–398, https://doi.org/10.1016/j.biortech.2015.07.099.

[75] M. Wilk, A. Magdziarz, K. Jayaraman, M. Szymańska-Chargot, I. Gökalp, Hydrothermal carbonization characteristics of sewage sludge and lignocellulosic biomass. A comparative study, Biomass Bioenerg 120 (2019) 166–175, https://doi.org/10.1016/j.biombioe.2018.11.016.

[76] J. Jia, B. Yu, L.M. Wu, H.W. Wang, Z.L. Wu, M. Li, P.Y. Huang, S.Q. Feng, P. Chen, Y.L. Zheng, L.C. Peng, Biomass enzymatic saccharification is determined by the non-KOH-extractable wall polymer features that predominately affect cellulose crystallinity in corn, PloS One 9 (9) (2014) e108449, https://doi.org/10.1371/journal.pone.0108449.